Sensors and Actuators B 174 (2012) 427–435

Contents lists available at SciVerse ScienceDirect

Sensors and Actuators B: Chemical

journal homepage: www.elsevier.com/locate/snb

Multi-functionalized biosensor at WO_3–TiO_2 modified electrode for photoelectrocatalysis of norepinephrine and riboflavin

Ying Li, Pei-Chi Hsu, Shen-Ming Chen*

Department of Chemical Engineering and Biotechnology, National Taipei University of Technology, No.1, Section 3, Chung-Hsiao East Road, Taipei 106, Taiwan, ROC

ARTICLE INFO

Article history:
Received 21 March 2012
Received in revised form 17 June 2012
Accepted 22 June 2012
Available online xxx

Keywords:
Titanium dioxide (TiO_2)
Tungsten oxide (WO_3)
Norepinephrine (NEP)
Riboflavin (Vitamin B2)
Modified electrodes
Photoelectrocatalysis

ABSTRACT

The titanium dioxide (TiO_2), mixed different ratio tungsten oxide (WO_3) hybrid film WO_3–TiO_2 was prepared on indium tin oxide (ITO) electrode. TiO_2:WO_3 = 9:3 (v/v) group current value was 5.44 mA under irradiation conditions. This group showed highest photocatalytic activity than others, we selected to optimization us in follow-up experiment. In this paper, the electrochemical oxidation and reduction of norepinephrine (NEP) and riboflavin (Vitamin B2) as multi-functionalized biosensor. The TiO_2 exhibited a promising enhanced photoelectrocatalytic activity toward analytes. Surface morphology of the modified electrode using atomic force microscopy (AFM), which revealed that WO_3 and TiO_2 were coated on ITO. The presence of TiO_2 enhances the loaded and stability. Electrochemical impedance spectroscopy (EIS) applied diffusion coefficient values and some information about the kinetics of electron transfer during the redox reactions. Cyclic voltammograms (CVs) and differential pulse voltammetry (DPVs) were used for the determination of analytes. DPVs not only increased the electrocatalytic current linear concentration range, also lowered the overpotential to oxidation or reduction the interferences in the measurements. We simulated more complex system if both norepinephrine and riboflavin are present simultaneously. It also exhibited oxidation and reduction peaks for norepinephrine injection and B complex tablet's real samples determination in pH 7.0 at WO_3–TiO_2 modified electrode.

1. Introduction

Titania (TiO_2) has attracted much attention as a photocatalyst for degradation of organic contaminations, due to its low cost, strong oxidizing power, non-toxicity, photo-stability and chemical inertness [1,2]. TiO_2 is one of these semiconductors which only exhibits its photocatalytic properties under UV illumination due to its relatively wide band gap (~3.2 eV). Its wide band gap means that it only absorbs in the UV region of the solar spectrum which represents only 4% of the incoming solar energy. It is necessary to alter TiO_2 surface structure and composition in order to improve its photoactivity under visible irradiation, because UV irradiation cannot be applied for a long time in practical applications. However, practically technological application of pure TiO_2 film is limited by easy recombination of photo-induced hole–electron pairs. In addition, its relatively high recombination rate of e^-–h^+ pairs adversely influences the photocatalytic activity [3,4]. Coupling TiO_2 with other semiconductor is considered as a good way because coupling two semiconductors with different redox energy levels can increase the charge separation for their corresponding conduction and valence bands [5]. A number of researches have been focused on the formation of TiO_2 films because of its reusability. Different solutions have been proposed to increase the absorption capacity of TiO_2 under the visible illumination and decrease the e^-–h^+ recombination rate. One of the most important solutions to defeat the suggested problems is coupling titania with other semiconductors, metallic, and nonmetallic species [6–15].

Tungsten oxide (WO_3) is an n-type semiconductor material, which has been regarded as promising applications in the information display devices and highly sensitive optical memory materials, since its photochromic properties were discovered [16]. WO_3 coatings have attracted vast interest for their possible application in catalysts [17], electrochromic (EC) devices [18–22], gasochromic coatings [23,24], gas sensors [25,26], photocatalysis [27–29] and batteries [30,31]. Recently, the synthesis of nanostructured WO_3 including nanoparticles, nanoplates, nanowires, nanorod bundles, nanoclusters and so forth [32–40], has been widely studied because of the obvious improvement in various properties. However, much less attention has been paid to the morphology improvement of WO_3 particles by small molecular organics so far. Therefore, to achieve fast and sufficient intercalation of ions, high surface ratio of films such as nanostructured or porous films is required [41–44]. Just as many fundamental properties and applications of materials depending not only on their shape and size, but also on their spatial orientation and arrangement of the nanocrystals, the morphologies of WO_3 units determine the performance

* Corresponding author. Tel.: +886 2270 17147; fax: +886 2270 25238.
E-mail address: smchen78@ms15.hinet.net (S.-M. Chen).

0925-4005/$ – see front matter © 2012 Elsevier B.V. All rights reserved.
http://dx.doi.org/10.1016/j.snb.2012.06.061

of these devices to a large extent [45]. Actually, a high surface ratio is also very helpful to applications such as sensors and photocatalysis. It is of great importance to prepare WO_3 with well-controlled dimensionality, sizes and crystal structure for basic research, so that many researches have been devoted to the fabrication of WO_3 nanostructures with various morphologies by different methods, including sol–gel [46–55], template method [56,57], anodic oxidation [58,59], gas evaporation, chemical vapor deposition (CVD) [60,61], thermal or electron beam evaporation [62–66], electrospinning [67], atmospheric pressure plasma jet [68], sputtering [69–73], electrodeposition [74–79], etc. and so on [80,81].

In recent years, several approaches of W doping have been developed to improve photocatalytic activity of TiO_2, it was found that the photocatalytic activity in visible light of TiO_2 nanopowders produced by flame spray synthesis (FSS) was enhanced significantly by the W-doping as well as by additional thermal treatment of those nanopowders [82]. It has been already demonstrated that the photocatalytic activity of the TiO_2 layers is enhanced when it is combined with WO_3. Three reasons have been put forward for this behavior. Once optical excitation takes place in the WO_3–TiO_2 composite layers, the photo-generated electrons can be transferred to the lower lying conduction band of WO_3, while the positive holes moves to ward the valence band of TiO_2 and accumulate there resulting in reduction of the electron–hole recombination rate and consequently photocatalytic activity enhancement. WO_3 is an appropriate material to couple with TiO_2 because WO_3 has a suitable conduction band potential to allow the transfer of photogenerated electrons from TiO_2 facilitating effective charge separation [83]. It has also demonstrated that the surface of WO_3–TiO_2 layers is more acidic than that of pure TiO_2. The increased acidity can generate a higher affinity of WO_3–TiO_2 layers for species with unpaired electrons; therefore, these films could absorb more OH^- or H_2O, and create more OH radical necessary for photo-oxidation reactions. Furthermore, due to the lower band gap energy, the light absorption capacity of the WO_3–TiO_2 systems is higher than that of the TiO_2 layers. It results in generation of more e^- and h^+ pairs [84–87].

In this study, we focus on the preparation of WO_3–TiO_2 composite film. The different concentration of WO_3 on the microstructure, photophysical properties and photocatalytic activity of the oxide films were investigated. We discussed the electrochemical of WO_3–TiO_2 films on various electrodes, and the enhancement of the photocatalytic reaction by WO_3 modification of the electrode surface as showed Scheme 1. It was interesting to study the electrochemical oxidation in different pHs and conditions. The formed films were classified and recognized by cyclic voltammograms (CVs) and atomic force microscopy (AFM) images. They were compared with bare ITO and WO_3–TiO_2/ITO for determination of norepinephrine (NEP) and riboflavin (Vitamin B2).

2. Experimental

2.1. Materials

P25 TiO_2 powder, Triton X-100 solution, acetylacetone, PEG 20000, norepinephrine (NEP) and riboflavin (Vitamin B2) were purchased from Sigma–Aldrich (USA). Indium tin oxide (ITO) (7 Ω/cm^{-2}) was purchased from Merck Display Technologies (MDT) Ltd. (Taiwan). All other chemicals used were of analytical grade and used without further purification pH 7.0 (0.1 M Na_2HPO_4 and 0.1 M NaH_2PO_4). Phosphate buffer solutions (PBS) and pH 1.0 H_2SO_4 solutions were used as supporting electrolyte. Aqueous solutions were prepared using doubly distilled deionized (DI) water and then deaerated by purging with high purity nitrogen gas for about 20 min

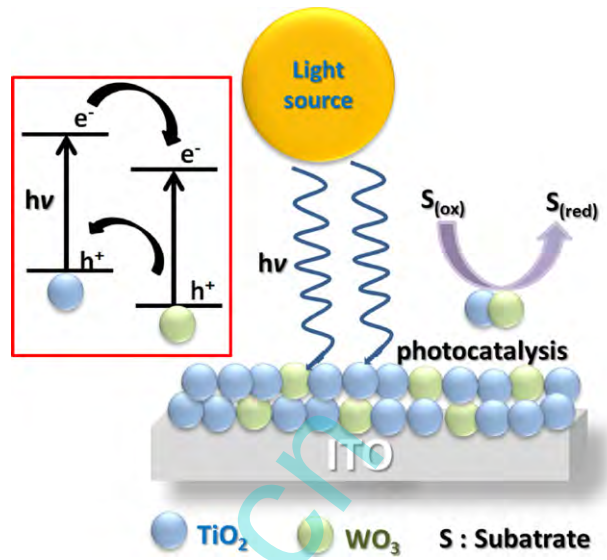

Scheme 1. Photoelectrocatalytic reaction of WO_3–TiO_2 modified electrodes.

before performing electrochemical experiments. Also, a continuous flow of nitrogen over the aqueous solution was maintained during measurements.

2.2. Apparatus

Cyclic voltammetry (CVs) was performed in an analytical system model CHI-1205A, differential pulse voltammetry (DPVs) were CHI-900 and CHI-410 potentiostat. A conventional three-electrode cell assembly consisting of an Ag/AgCl reference electrode and a Pt wire counter electrode were used for the electrochemical measurements. The working electrode was Indium tin oxide (ITO) (area $1 \times 1\,cm^2$). In these experiments, all the potentials have been reported vs. the Ag/AgCl reference electrode. The morphological characterizations of the films were examined by atomic force microscopy (Being Nano-Instruments CSPM 5000). Electrochemical impedance spectroscopy (EIS) measurements were performed using an IM6ex Zahner instrument (Kroanch, Germany). The power output measurements system by KEITHLEY 2400 with full sunlight of 100 mW cm^{-2} (AM 1.5) conditions. All the experiments were carried out at room temperature (≈25 °C).

2.3. Preparation of WO_3–TiO_2/ITO modified electrodes

Nano TiO_2 films on ITO substrates were deposited as follows, 9 g P-25 TiO_2 powder with different ratio of WO_3, 25 μl Triton X-100, 1 g PEG 20000, 50 μl acetylacetone and 18 ml DI water were mixed well in a dried agate mortar for 1 h. The final mixture was stirred for an additional 2 days to obtain the desired WO_3–TiO_2 paste (TiO_2:WO_3 = 9:0, 9:1, 9:3, 9:5, 9:7, 9:9 and 0:9 v/v). In prior to modification, ITO surfaces were cleaned and ultrasonicated in acetone–water mixture for 15 min and then dried. The above obtained WO_3–TiO_2 paste solution was spin-coated on an ITO glass substrate at 1000 rpm for 10 s and 2000 rpm for 30 s. The formed film was annealed at 450 °C for 1 h in atmosphere. These WO_3–TiO_2 film coated on ITO were dried at room temperature for cooling several minutes.

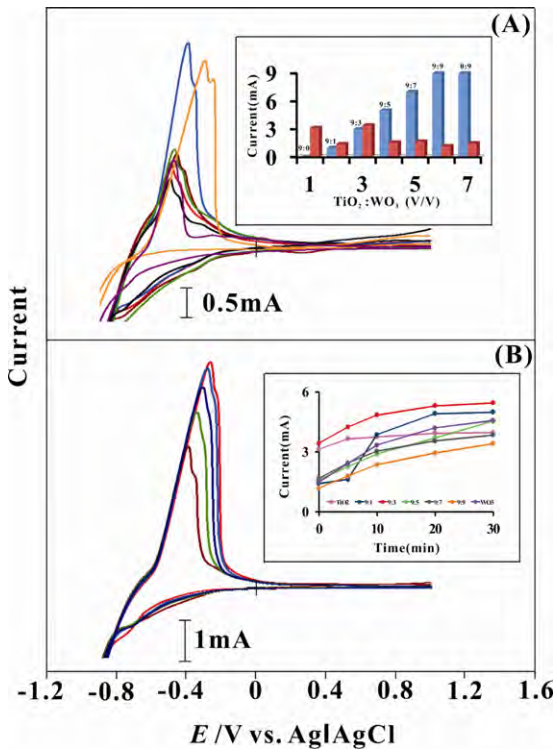

Fig. 1. (A) Cyclic voltammograms of catalytic activity with WO_3–TiO_2/ITO modified electrodes embedded with different contents of WO_3 in TiO_2 film were examined at same time. The insert displayed different concentration WO_3 and response current. (B) showed that CVs of TiO_2:WO_3 = 9:3 groups under different irradiation conditions from 0 to 30 min. The insert displayed all groups of response current and different irradiation conditions.

3. Results and discussions

3.1. Electrochemical characterizations of different ratio WO_3–TiO_2

To investigate the effects of WO_3 content on the performances of sensor, a series of working electrodes were prepared from the mixtures with different contents of WO_3. The electrocatalytic efficiency of WO_3–TiO_2/ITO modified electrodes in the presence of different concentration WO_3 (TiO_2: WO_3 = 9:0, 9:1, 9:3, 9:5, 9:7, 9:9 and 0:9 v/v) in pH 1.0 H_2SO_4 solutions using cyclic voltammetry. Fig. 1(A) showed that the performances of the catalytic activity with WO_3–TiO_2/ITO modified electrodes embedded with different contents of WO_3 in TiO_2 film were examined at same time. The insert displayed different concentration WO_3 and response current. Initial reaction, TiO_2:WO_3 = 9:0 and 9:3 groups of current value were 3.12 and 3.42 mA. These groups were exhibited higher current then others. TiO_2 showed broad background current under 0 min conditions. In the same conditions, TiO_2:WO_3 = 9:9 group of current value was 1.17 mA. This group was unfavorable to next experiment. Fig. 1(B) showed that CVs of TiO_2:WO_3 = 9:3 groups under different irradiation conditions from 0 to 30 min. The insert displayed all groups of response current and different irradiation conditions. All groups of current in each irradiation conditions reveals that the current value increased as the irradiation time was increased. Under irradiation 30 min conditions, TiO_2:WO_3 = 9:0 current value was 3.95 mA. Compared with current previously, TiO_2:WO_3 = 9:0 group of irradiation rised to slight breadth. However, TiO_2:WO_3 = 9:3 group current value was 5.44 mA. This group showed highest photocatalytic activity than others, we selected to optimization us in follow-up experiment. All results showed individual current value in different irradiation conditions with variance ratio WO_3 as in Table 1.

Table 1
Different irradiation conditions with variance ratio TiO_2/WO_3.

TiO_2 (ml)	WO_3 (ml)	Irradiation/current (mA)				
		Time (min)				
		0	5	10	20	30
9	0	3.126	3.645	3.754	3.926	3.957
9	1	1.412	1.615	3.848	4.909	4.985
9	3	3.422	4.231	4.836	5.302	5.447
9	5	1.582	2.243	2.883	3.699	4.526
9	7	1.66	2.432	3.029	3.547	3.838
9	9	1.172	1.781	2.35	2.935	3.416
0	9	1.477	2.412	3.329	4.186	4.566

3.2. Morphological characterization of WO_3–TiO_2 modified electrodes

The surface morphology of WO_3–TiO_2 modified electrode has been examined using AFM. Here the AFM studies could furnish the comprehensive information about the surface morphology of nanostructure on the ITO surface. The AFM parameters have been evaluated for 13,000 × 13,000 nm and 19,000 × 19,000 nm surface area. Further, three different films; TiO_2, WO_3 and WO_3–TiO_2 modified electrodes have been prepared on ITO electrode were characterized using AFM. From Fig. 2, it is significant that there are morphological differences between both the films. The top views of nanostructures (A) shows uniformly deposited homogeneously dispersed TiO_2 on electrode. We observed the existence of nanostructures in obvious manner with the average size range of 76.2 nm. By AFM section analysis, the other amplitude parameters such like roughness average (sa) for TiO_2 film (13,000 × 13,000 nm) was found as 1.09 nm. The root mean square roughness was found as 1.53 nm. The WO_3 film in Fig. 2(B) showed average size range of 224 nm. From section analysis, roughness average (sa) for WO_3 film (190,000 × 190,000 nm) was found as 5.55 nm. The root mean square roughness was found as 8.47 nm. WO_3 exhibited more large particle size than others. Fig. 2(C) showed WO_3–TiO_2 film (110,000 × 110,000 nm), average size range and roughness average (sa) were 51.5 and 1.26 nm. The root mean square roughness of WO_3–TiO_2 was found as 1.78 nm. Comparison of only WO_3 (B) and WO_3–TiO_2 (C) reveals, these results in could be explained as the small particle size of WO_3 in presence TiO_2. We can clearly see that the WO_3–TiO_2 have been gathered together.

3.3. Electrochemical impedance spectra (EIS) of WO_3–TiO_2 modified electrodes

Electrochemical impedance spectra (EIS) can give useful information of the impedance changes on the electrode surface between each step and apply to monitor the whole process of the electrode modification. The EIS included a semicircular part and a linear part. From the shape of an impedance spectrum, the electron-transfer kinetics and diffusion characteristics can be extracted. The respective semicircle parameters correspond to the electron transfer resistance (R_{et}) and the double layer capacity (C_{dl}) nature of the modified electrode. The semicircular part at higher frequencies corresponds to the electron transfer limited process and the diameter is equivalent to the electron transfer resistance (R_{ct}). The linear part at lower frequencies corresponds to the diffusion process. The plot of the real component (Z') and the imaginary component Z'' (imaginary) resulted in the formation of a semicircular Nyquist plot. This type of impedance spectrum is an analytic of a surface-modified electrode system in which the electron transfer is slow and the

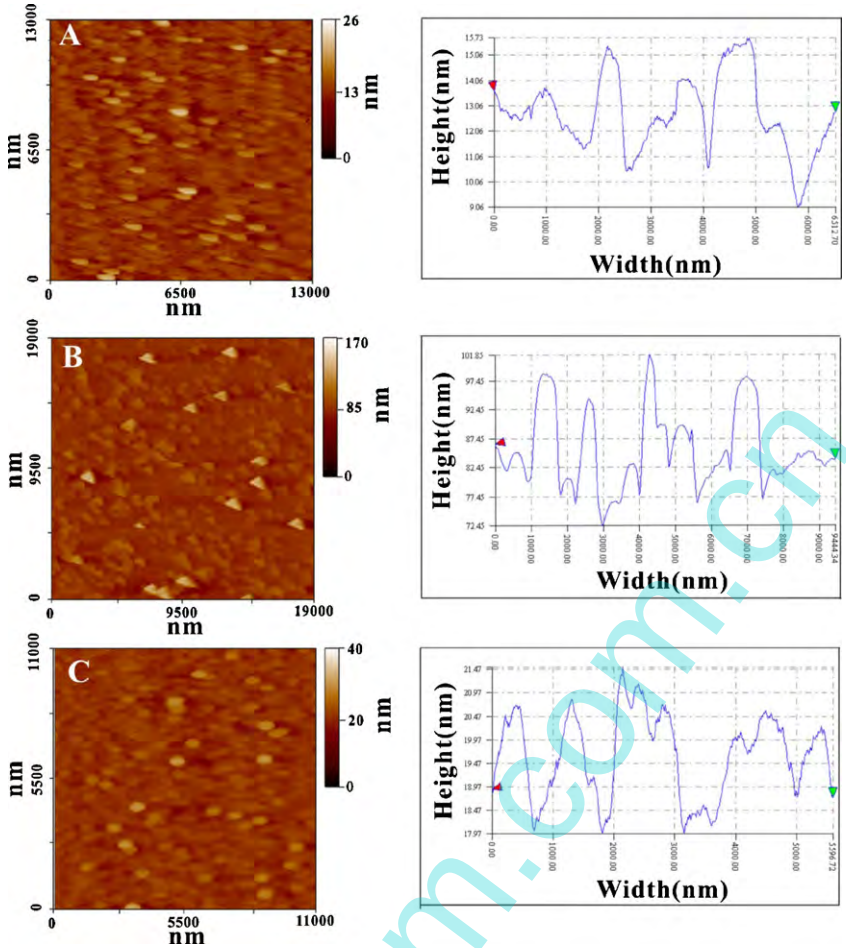

Fig. 2. AFM images and section analysis of (A) only TiO_2, (B) only WO_3 and (C) WO_3–TiO_2 on ITO electrode.

impedance is controlled by the interfacial electron transfer at high frequency. Open circuit potential was applied for this investigation. Fig. 3 showed the results of EIS for different modified electrodes in the presence pH 7.0 PBS of equimolar 5 mM $[Fe(CN)_6]^{3-/4-}$. Fig. 3 showed the Faradaic impedance spectra, presented as Nyquist plots (Z'' vs. Z') for the TiO_2, WO_3 and WO_3–TiO_2 modified electrodes. The TiO_2 exhibited almost a straight line (curve c) with a very small depressed semicircle arc (R_{et} = 213 (Z'/Ω)) represents the characteristics of diffusion limited electron-transfer process on the electrode surface. At the same time, the WO_3 modified electrode showed like a depressed semicircle arc with an interfacial resistance due to the electrostatic repulsion between the charged surface and probe molecule $Fe(CN)_6^{-3/-4}$ (curve b). This depressed semicircle arc (R_{et} = 323 (Z'/Ω)) clearly indicated the higher electron transfer resistance behavior comparing with the TiO_2 electrode. WO_3–TiO_2 (curve c) modified electrodes's R_{et} had been found as 465 (Z'/Ω). The insert displayed the equivalent circuit (Randles model) was used to fit Nyquist diagrams. It constitutes a distributed element which can only be approximated by an infinite series of simple electrical elements. From AFM results, the TiO_2 and WO_3 electrode of average size range were 76.2 nm and 224 nm. We supposed that the increased in the value of electron transfer resistance (R_{et}) due to the embeddedness of WO_3. In contrast, the dispersed WO_3 adversely influences electron transfer resistance performance, since its photocatalytic activity is significantly weaker than that of TiO_2.

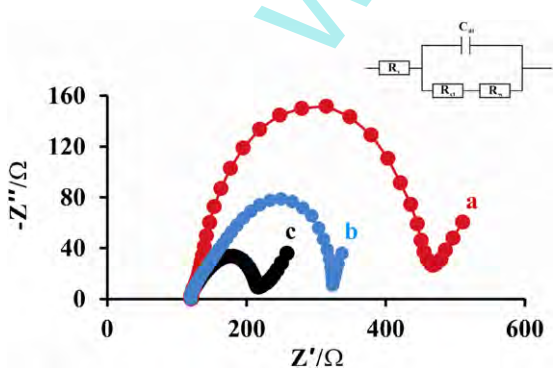

Fig. 3. Electrochemical impedance spectra (EIS) of different modified electrodes in pH 7.0 PBS containing 5×10^{-3} M $[Fe(CN)_6]^{-3/-4}$, amplitude: 5 mV. (a) WO_3–TiO_2, (b) WO_3 and (c) TiO_2 on ITO electrode. The insert displayed equivalent circuit.

3.4. Electrochemical characterizations of WO_3–TiO_2 modified electrode in different pH

Fig. 4(A) showed the cyclic voltammetric of WO_3–TiO_2 modified electrode transferred to various pH aqueous buffer solutions. This was displayed that the WO_3–TiO_2 modified electrode had highly stable in the pH range between 1 and 13 (curve a–g). All showed one reversible redox couple at potentials between −0.4 and −1.6 V (vs. Ag/AgCl). The values of *E*pa and *E*pc depends on the pH value of the buffer solution. From different pH, a peak of WO_3–TiO_2 shows a pH-dependent response, which indicates that protons were involved in the electron-transfer reaction. WO_3–TiO_2 modified electrode on ITO that surface nanoparticles layers instead of direct current improves the protons efficiency. Fig. 4(B) showed

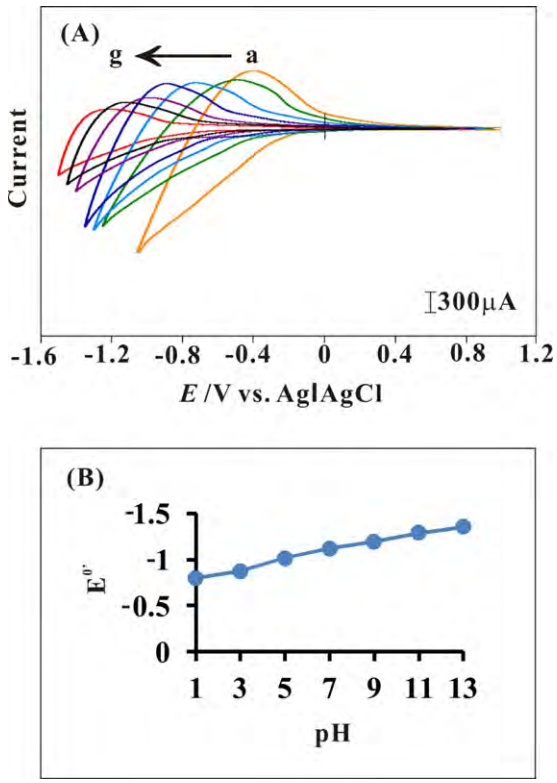

Fig. 4. (A) Cyclic voltammograms of WO_3–TiO_2 modified electrodes transferred to various pH solutions (a) 1, (b) 3, (b) 5, (d) 7, (e) 11 and (f) 13. Scan rate 100 mV s^{-1}. (B) The inset showed the plot of formal potential ($E^{0\prime}$) vs. pH.

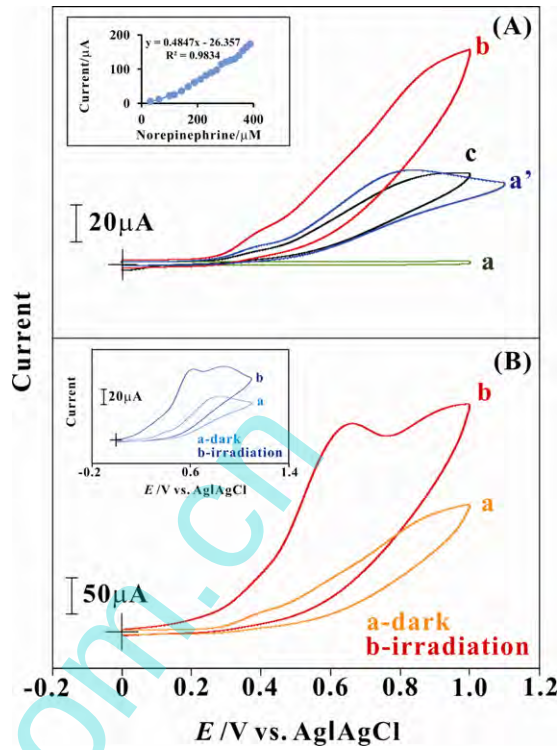

Fig. 5. (A) Electrocatalytic detection by cyclic voltammograms of (a′) bare ITO electrode, (b) WO_3–TiO_2 and (c) TiO_2 examined in PBS (pH 7.0) containing 3.88×10^{-4} M norepinephrine, (a) WO_3–TiO_2 in the absence of norepinephrine, scan rate = 100 mV s^{-1}. The insert displayed WO_3–TiO_2 modified electrode after various norepinephrine concentration additions. (B) A typical photocurrent response of WO_3–TiO_2 modified electrode in PBS (pH 7.0) containing 3.88×10^{-4} M norepinephrine with scan rate 100 mV s^{-1} under (a) dark and (b) illumination (light source, Xe lamp 100 mW cm^{-2}). The inset showed the bare ITO electrode in the same condition absence (a) and presence (b) illumination.

the potential of WO_3–TiO_2 plotted over a pH range from 1 to 13. In low pH (pH 1.0, curve a) response of oxidation process resulted in irreversible oxidation peak about −0.79 V. Curve (b)–(g) in pH 3.0–13 showed that the peak potentials shifted to the negative potentials by increasing pH. As increasing pH the peak current declined. Exhibited of oxidation process produced reversible redox peak. It has also demonstrated that the surface of WO_3–TiO_2 layers is more acidic than that of pure TiO_2. The increased acidity can generate a higher affinity of WO_3–TiO_2 layers for species with unpaired electrons; therefore, these films could absorb more OH^- or H_2O, and create more OH radical necessary for photo-oxidation reactions. Furthermore, due to the lower band gap energy, the light absorption capacity of the WO_3–TiO_2 systems is higher than that of the TiO_2 layers. It results in generation of more e^- and h^+ pairs.

3.5. Photoelectrocatalytic detection of norepinephrine and riboflavin at WO_3–TiO_2 modified electrode

The electrocatalytic reaction of norepinephrine was examined at WO_3–TiO_2 modified electrode with the potential range of 0–1.0 V and the scan rate of 100 mV s^{-1} in 0.1 M PBS (pH 7.0). Fig. 5(A) showed the cyclic voltammogram of WO_3–TiO_2 modified electrode obtained in the absence (blank, curve a) and presence (curve b) of the 3.88×10^{-4} M norepinephrine. Compared with TiO_2 (curve c) and bare (curve a′) ITO electrode examined in the same concentration of norepinephrine, the WO_3–TiO_2 modified electrode (curve b) exhibited a redox couple ($E^{0\prime}$ = 0.83 V) and a higher peak current response to norepinephrine. It was obvious that the WO_3–TiO_2 modified electrode showed higher electrocatalytic activity then TiO_2 and bare ITO electrode for norepinephrine. This peak current response occurs due to the reaction mechanism of norepinephrine oxidation. Whereas Fig. 5(A) the insert displayed the CVs obtained at the same WO_3–TiO_2 modified electrode after various norepinephrine concentration additions. The catalytic current response can be directly proportional to norepinephrine concentration if increasing the norepinephrine content in the system. Above these results validated that the WO_3–TiO_2 modified electrode was capable for the electrocatalytic response of norepinephrine with detection limit of 1.07×10^{-6} M (S/N = 3). From this calibration plot, the linear concentration range was obtained as 3.23×10^{-6} to 3.88×10^{-4} M, respectively. As the result, this electrode is found stable and electroactive for the electrocatalytic oxidation of norepinephrine.

The photoelectrocatalytic activity of WO_3–TiO_2 modified electrode towards norepinephrine has been investigated using CVs experiments in Fig. 5(B). A typical photocurrent response of WO_3–TiO_2 modified electrode with scan rate 100 mV s^{-1} under illumination (light source, Xe lamp 100 mW cm^{-2}). As the figure indicated, a broad background current was first observed for the response of TiO_2. With the injection of a higher norepinephrine concentration, the photocurrent increased with the increased of analytes. Curve (a) was WO_3–TiO_2 modified electrode in 3.88×10^{-4} M norepinephrine in pH 7.0 PBS under dark conditions; curve (b) was under irradiation conditions. Comparison of them, it was found increased the photocatalytic effect of peak currents under illumination. The inset of Fig. 5(B) showed the bare ITO electrode in 3.88×10^{-4} M norepinephrine pH 7.0 PBS absence (curve a) and presence (curve b) illumination. It was obvious that the WO_3–TiO_2 modified electrode showed higher electrocatalytic activity then bare ITO electrode for norepinephrine. WO_3–TiO_2 modified electrode in the presence of norepinephrine showed two anodic peak, we supposed that norepinephrine was photosensitive.

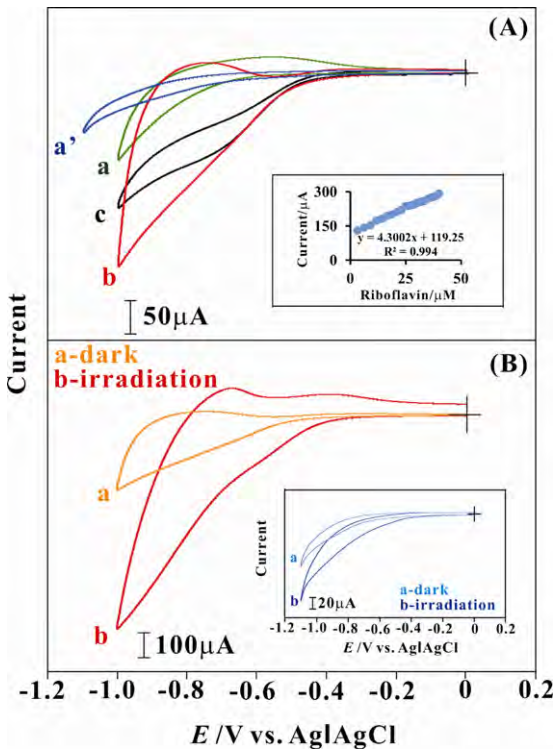

Fig. 6. (A) Electrocatalytic detection by cyclic voltammograms of (a′) bare ITO electrode, (b) WO_3–TiO_2 and (c) TiO_2 examined in PBS (pH 7.0) containing 4.0×10^{-5} M riboflavin, (a) WO_3–TiO_2 in the absence of riboflavin, scan rate = 100 mV s^{-1}. The insert displayed WO_3–TiO_2 modified electrode after various riboflavin concentration additions. (B) A typical photocurrent response of WO_3–TiO_2 modified electrode in PBS (pH 7.0) containing 4.0×10^{-5} M riboflavin with scan rate 100 mV s^{-1} under (a) dark and (b) illumination (light source, Xe lamp 100 mW cm^{-2}). The inset showed the bare ITO electrode in the same condition absence (a) and presence (b) illumination.

From inset indicated bare electrode in the presence of norepinephrine showed two anodic weaker current at 0.4 V and 0.8 V despite under dark conditions. More specifically, the enhanced electrocatalysis of WO_3–TiO_2 modified electrode can be explained in terms of higher peak current and lower overpotential by TiO_2 under illumination.

Fig. 6(A) displayed the CVs of catalytic reduction at different types modified electrode, WO_3–TiO_2 modified electrode without addition of riboflavin (blank, curve a); WO_3–TiO_2 modified electrode (curve b), TiO_2 (curve c) and bare ITO electrode (curve a′) presence of 4.0×10^{-5} M riboflavin in pH 7.0 PBS at the scan rate of 100 mV s^{-1}. It can be seen that a small response was observed for bare ITO electrode (curve a′) at potential range 0 to −1.0 V in the presence of riboflavin, but the WO_3–TiO_2 modified electrode (curve b) showed a remarkable increase current in the same condition. The reduction catalytic current of riboflavin at potential of −1.0 V. TiO_2 can dramatically enhance the electrochemical response of WO_3, resulting in increasing redox currents. Whereas the insert obtained of CVs at the same WO_3–TiO_2 modified electrode after various riboflavin concentration additions. The reduction catalytic current response increasing by riboflavin concentration increasing in the system. Above these results validated that the WO_3–TiO_2 modified electrode was capable for the electrocatalytic response of riboflavin with detection limit of 1.87×10^{-7} M (S/N = 3). From this calibration plot, the linear concentration range from 3.23×10^{-7} to 4.0×10^{-5} M, respectively. As the result, this electrode is found stable and electroactive for the electrocatalytic reduction of riboflavin. Fig. 6(B) showed photoelectrocatalytic activity of WO_3–TiO_2 modified electrode reduction of riboflavin by CVs. A typical photocurrent response of WO_3–TiO_2 modified electrode with scan rate 100 mV s^{-1} under illumination. With the injection of a higher riboflavin concentration, the photocurrent increased by the increased of analytes. Curve (a) was WO_3–TiO_2 modified electrode in 4.0×10^{-5} M riboflavin pH 7.0 PBS under dark conditions; curve (b) was under irradiation conditions. Comparison of them, it was found increased the photocatalytic effect of peak currents under illumination. The inset of Fig. 6 (B) showed the bare ITO electrode in 4.0×10^{-4} M riboflavin in pH 7.0 PBS absence (curve a) and presence (curve b) illumination. It was obvious that the WO_3–TiO_2 modified electrode showed higher electrocatalytic activity then bare ITO electrode for riboflavin. More specifically, the enhanced electrocatalysis of WO_3–TiO_2 modified electrode can be explained in terms of higher peak current by TiO_2 under illumination. This observation illustrated that TiO_2 played significant role to photoelectrocatalysis of norepinephrine and riboflavin on the modified ITO electrode.

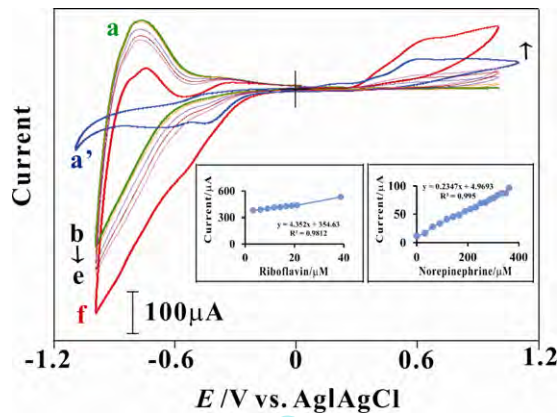

Fig. 7. Cyclic voltammograms of electrocatalytic oxidation and reaction of mixture was obtained in the absence (blank, curve a), bare (curve a′) and presence (curve b–f) of various concentration mixture at WO_3–TiO_2 modified electrode with the potential range of −1.0 to 1.0 V and the scan rate of 100 mV s^{-1} in 0.1 M PBS (pH 7.0). The inserts displayed various concentration mixture additions.

3.6. Complex system and real samples determination of norepinephrine and riboflavin simultaneously

We simulated more complex system if both norepinephrine and riboflavin were present simultaneously. The electrocatalytic oxidation and reaction of mixture was examined at WO_3–TiO_2 modified electrode with the potential range of −1.0 to 1.0 V and the scan rate of 100 mV s^{-1} in 0.1 M PBS (pH 7.0). Fig. 7 showed the cyclic voltammogram of WO_3–TiO_2 modified electrode obtained in the absence (blank, curve a) and presence (curve b–f) of various concentration mixture. Compared with bare (curve a′) ITO electrode examined in the highest concentration of mixture, the WO_3–TiO_2 modified electrode (curve f) exhibited a higher peak current response. It was obvious that the WO_3–TiO_2 modified electrode showed higher electrocatalytic activity then bare ITO electrode for mixture. The inserts displayed the CVs obtained at the same WO_3–TiO_2 modified electrode after various concentration mixture additions. It also exhibited oxidation and reduction peaks for norepinephrine and riboflavin real samples determination at WO_3–TiO_2 modified electrode. CVs of electrocatalytical values obtained for the norepinephrine injection and B complex tablet's determination in pH 7.0 Normal Saline (0.9%). Norepinephrine injection were obtained from Levophed®. The injection labeled composition is 1 mg/mL norepinephrine HCl. B complex tablet were obtained from Nature Made®. The tablet labeled composition is 24 mg of riboflavin, protein 0.12 g, fat 0.02 g, carbohydrate 0.22 g, vitamins B1 24 mg, vitamins B6 20 mg, vitamins B12 30 mg, vitamins B5

Table 2
Cyclic voltammograms of electrocatalytical values obtained for the norepinephrine injection and B complex tablet's determination in pH 7.0 Normal Saline (0.9%) at WO_3–TiO_2 modified electrode.

Analytes	Added (μM)	Found (μM)	RSD (%)	Recover (%)
	5	5.02	1.98	102
	25	25.17	2.76	105.6
NEP[a]	100	100.46	1.28	107
	200	201.8	2.34	108
	300	307.6	1.76	109
	0.5	0.5011	1.98	100.5
	2.5	2.508	1.73	102
B2[b]	10	10.73	2.82	103
	20	20.61	2.44	103.8
	30	30.85	2.57	105

[a] Norepinephrine injection from Levophed®.
[b] B complex tablet from Nature Made®.

20 mg, folic acid 400 mg, biotin 60 mg and others. In these experiments, the concentration added, found and the relative standard deviation (RSD) were given in Table 2. From these results, the recovery of norepinephrine was ≈105% and riboflavin was ≈102%. These above results show that WO_3–TiO_2 modified electrode was efficient for real sample detection. Above these results validated that the WO_3–TiO_2 modified electrode was multi-functionalized biosensor.

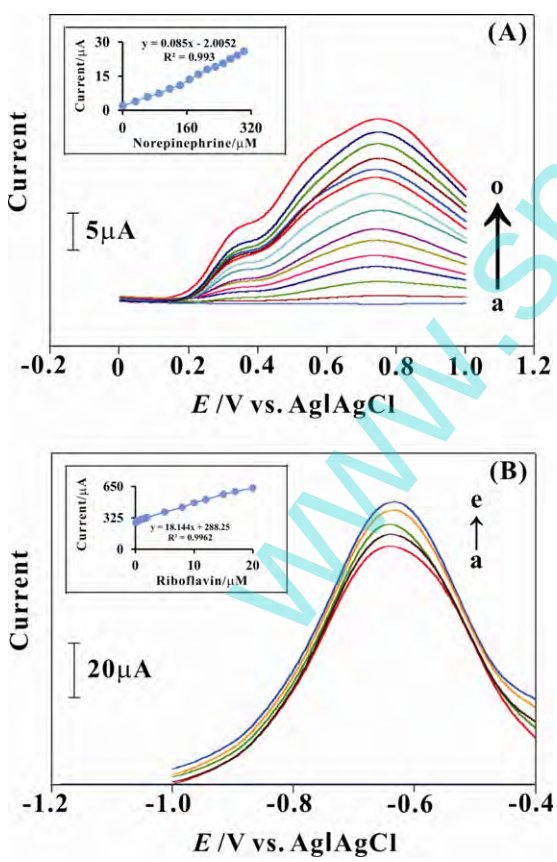

Fig. 8. (A) Differential pulse voltammetry (DPVs) of different concentrations (a–o) norepinephrine at WO_3–TiO_2 modified electrode. They demonstrate the calibration curves for analyte, which are almost linear for concentrations range 1.89×10^{-7} to 3.18×10^{-4} M as shown in inset, respectively. (B) DPVs of different concentrations (a–e) riboflavin at WO_3–TiO_2 modified electrode. They demonstrate the calibration curves for analyte, which are almost linear for concentrations range 3.12×10^{-8} to 2.0×10^{-5} M as shown in inset.

3.7. Differential pulse voltammetry (DPVs) of norepinephrine and riboflavin at WO_3–TiO_2 modified electrode

The Differential pulse voltammetry of have been obtained different concentrations (a–o) of norepinephrine at WO_3–TiO_2 modified electrode, as shown in Fig. 8(A). The DPVs had been recorded at a constant time interval of 2 min with nitrogen purging before the start of each experiment. Interestingly, the peak currents for norepinephrine increased linearly with the increased of analyte concentration. They demonstrate the calibration curves for analyte, which are almost linear for a wide range of concentrations as shown in inset. From this calibration plot, the linear concentration range was obtained as 1.89×10^{-7} to 3.18×10^{-4} M, respectively. The electrocatalytic activity exhibited a redox couple at 0.75 V.

Fig. 8(B) showed the DPVs of different concentrations riboflavin (a–e) at WO_3–TiO_2 modified electrode. The reduction of current for riboflavin increased linearly with the increased of analyte concentration. They demonstrate the calibration curves for analyte, which are almost linear for a wide range of concentrations as showed in inset. From this calibration plot, the linear concentration range was obtained as 3.12×10^{-8} to 2.0×10^{-5} M, respectively. The electrocatalytic activity exhibited a redox couple at −0.65 V. DPVs not only increased the electrocatalytic current linear concentration range, also lowered the overpotential to oxidation or reduction the interferences in the measurements.

4. Conclusions

We have demonstrated application of the WO_3–TiO_2 modified electrode for determination of norepinephrine (NEP) and riboflavin (Vitamin B2) simultaneously. This feature provides a favorable clinical diagnosis for multi-functionalized biosensor. TiO_2:WO_3 = 9:3 group showed highest photocatalytic activity than others, researcher can select to optimization as sustainable model. High stability and convenient together with very easy preparation WO_3–TiO_2 modified electrode as promising candidate for constructing simple electrochemical biosensor for norepinephrine and riboflavin determination. The experimental methods of cyclic voltammetry (CVs) and differential pulse voltammetry with biosensor integrated into the WO_3–TiO_2 modified electrode which are presented in this paper, provide an opportunity for qualitative and quantitative characterization, even at physiologically relevant conditions. The AFM results showed the difference between WO_3, TiO_2 and WO_3–TiO_2 modified electrode morphological data. Therefore, this work establishes and illustrates, in principle and potential, a simple and novel approach for the development of a biosensor which was based on the transparent electrode or ITO electrode.

Acknowledgement

This work was supported by the National Science Council of the Taiwan (ROC).

References

[1] G.H. Li, S. Ciston, Z.V. Saponjic, L. Chen, N.M. Dimitrijevic, T. Rajh, K.A. Gray, Synthesizing mixed-phase TiO_2 nanocomposites using a hydrothermal method for photo-oxidation and photoreduction applications, Journal of Catalysis 253 (2008) 105.
[2] S.S. Chin, K. Chiang, A.G. Fane, The stability of polymeric membranes in a TiO_2 photocatalysis process, Journal of Membrane Science 275 (2006) 202.
[3] A. Fujishima, X. Zhang, D.A. Tryk, TiO_2 photocatalysis and related surface phenomena, Surface Science Reports 63 (2008) 515.
[4] L. Li, C.Y. Liu, Y. Liu, Study on activities of vanadium (IV/V) doped TiO_2(R) nanorods induced by UV and visible light, Materials Chemistry and Physics 113 (2009) 551.
[5] L. Wu, J.C. Yu, X.Z. Fu, Characterization and photocatalytic mechanism of nanosized CdS coupled TiO_2 nanocrystals under visible light irradiation, Journal of Molecular Catalysis A: Chemical 244 (2006) 25.

[6] D. Robert, Photosensitization of TiO_2 by M_xO_y and M_xS_y nanoparticles for heterogeneous photocatalysis applications, Catalysis Today 122 (2007) 20.
[7] C. Gao, J. Li, Z. Shan, F. Huang, H. Shen, Preparation and visible-light photocatalytic activity of In_2S_3/TiO_2 composite, Materials Chemistry and Physics 122 (2010) 183.
[8] Q. Xiao, L. Ouyang, L. Gao, W. Jiang, One-step hydrothermal preparation and photocatalytic activity of (C, S, Sm)-tridoped mesoporous TiO_2 photocatalyst under visible light irradiation, Materials Chemistry and Physics 124 (2010) 1210.
[9] G.G. Nakhate, V.S. Nikam, K.G. Kanade, S. Arbuj, B.B. Kale, J.O. Baeg, Hydrothermally derived nanosized Ni-doped TiO_2: a visible light driven photocatalyst for methylene blue degradation, Materials Chemistry and Physics 124 (2010) 976.
[10] M.R. Bayati, A.Z. Moshfegh, F. Golestani-Fard, On the photocatalytic activity of the sulfur doped titania nano-porous films derived via microarc oxidation, Applied Catalysis A-General 389 (2010) 60.
[11] S.H. Kang, H.S. Kim, J.Y. Kim, Y.E. Sung, Enhanced photocurrent of nitrogen-doped TiO_2 film for dye-sensitized solar cells, Materials Chemistry and Physics 124 (2010) 422.
[12] N. Bahadur, K. Jain, A.K. Srivastava, Govind, R. Gakhar, D. Haranath, M.S. Dulat, Effect of nominal doping of Ag and Ni on the crystalline structure and photocatalytic properties of mesoporous titania, Materials Chemistry and Physics 124 (2010) 600.
[13] H. Wang, Z. Wang, H. Hong, Y. Yin, Preparation of cerium-doped TiO_2 film on 304 stainless steel and its bactericidal effect in the presence of sulfate-reducing bacteria (SRB), Materials Chemistry and Physics 124 (2010) 791.
[14] G. Cao, Y. Li, Q. Zhang, H. Wang, Synthesis and characterization of La_2O_3/TiO_2-*xFx* and the visible light photocatalytic oxidation of 4-chlorophenol, Journal of Hazardous Materials 178 (2010) 440.
[15] M.R. Bayati, A.Z. Moshfegh, F. Golestani-Fard, In situ growth of vanadia–titania nano/micro-porous layers with enhanced photocatalytic performance by micro-arc oxidation, Electrochimica Acta 55 (2010) 3093.
[16] N. Xu, M. Sun, Y.W. Cao, J.N. Yao, E.G. Wang, Influence of pH on structure and photochromic behavior of nanocrystalline WO_3 films, Applied Surface Science 157 (2000) 81.
[17] J.P. Chen, R.T. Yang, Role of WO_3 in mixed V_2O_5–WO_3/TiO_2 catalysts for selective catalytic reduction of nitricoxide with ammonia, Applied Catalysis A: General 80 (1992) 135.
[18] S.K. Deb, Opportunities and challenges in science and technology of WO_3 for electrochromic and related applications, Solar Energy Materials and Solar Cells 92 (2008) 245.
[19] G.A. Niklasson, C.G. Granqvist, Electrochromics for smart windows: thin films of tungsten oxide and nickel oxide, and devices based on these, Journal of Materials Chemistry 17 (2007) 127.
[20] C.G. Granqvist, P.C. Lansaker, N.R. Mlyuka, G.A. Niklasson, E. Avendano, Progress in chromogenics: new results for electrochromic and thermochromic materials and devices, Solar Energy Materials and Solar Cells 93 (2009) 2032.
[21] C.G. Granqvist, Oxide electrochromics: why, how, and whither, Solar Energy Materials and Solar Cells 92 (2008) 203.
[22] J. Zhang, J.P. Tu, X.H. Xia, Y. Qiao, Y. Lu, An all-solid-state electrochromic device basedonNiO/WO_3 complementary structure and solid hybrid poly-electrolyte, Solar Energy Materials and Solar Cells 93 (2009) 1840.
[23] M. Zayat, R. Reisfeld, H. Minti, B. Orel, F. Svegl, Gasochromic effect in platinum-doped tungsten trioxide films prepared by the sol–gel method, Journal of Sol-Gel Science and Technology 11 (1998) 161.
[24] D. Schweiger, A. Georg, W. Graf, V. Wittwer, Examination of the kinetics and performance of a catalytically switching (gasochromic) device, Solar Energy Materials and Solar Cells 54 (1998) 99.
[25] O.U. Nimittrakoolchai, S. Supothina, High-yield precipitation synthesis of tungsten oxide platelet particle and its ethylene gas-sensing characteristic, Materials Chemistry and Physics 112 (2008) 270.
[26] E. Gyorgy, G. Socol, I.N. Mihailescu, C. Ducu, S. Ciuca, Structural and optical characterization of WO_3 thin films for gas sensor applications, Journal of Applied Physics 97 (2005) 093527 (3 pp.).
[27] M. Sadakane, K. Sasaki, H. Kunioku, B. Ohtani, W. Ueda, R. Abe, Preparation of nano-structured crystalline tungsten (VI) oxide and enhanced photocatalytic activity for decomposition of organic compounds under visible light irradiation, Chemical Communications (2008) 6552.
[28] M. Shibuya, M. Miyauchi, Site-selective deposition of metal nanoparticles on aligned WO_3 nanotrees for super-hydrophilic thin films, Advanced Materials 21 (2009) 1373.
[29] S. Berger, H. Tsuchiya, A. Ghicov, P. Schmuki, High photocurrent conversion efficiency in self-organized porousWO3, Journal of Applied Physics 88 (2006) 203119 (3 pp.).
[30] A. Hauch, A. Georg, U.O. Krasovec, B. Orel, Photovoltaically self-charging battery, Journal of the Electrochemical Society 149 (2002) A1208.
[31] W.J. Li, Z.W. Fu, Nanostructured WO_3 thin film as a new anode material for lithium-ion batteries, Applied Surface Science 256 (2010) 2447.
[32] A.M. de la Cruz, D.S. Martínez, E.L. Cuéllar, Synthesis and characterization of WO_3 nanoparticles prepared by the precipitation method: evaluation of photocatalytic activity under vis-irradiation, Solid State Sciences 12 (2010) 92.
[33] R.H. Acuña, F.P. Delgado, M.A. Albiter, J.L. Romero, R.M. Sánchez, Synthesis and characterization of WO_3 nanostructures prepared by an aged hydrothermal method, Materials Characterization 60 (2009) 932.
[34] D. Meng, T. Yamazaki, Y. Shen, Z. Liu, T. Kikuta, Preparation of WO_3 nanoparticles and application to NO_2 sensor, Applied Surface Science 256 (2009) 1050.
[35] M. Laura, G. Tozzola, A. Tacca, G. Marra, S. Caramori, C. Vito, C.A. Bignozzi, Photo-electrochemical properties of nanostructured WO_3 prepared with different organic dispersing agents, Solar Energy Materials and Solar Cells 94 (2010) 788.
[36] S. Xintai, F. Xiao, Y. Li, J. Jian, Q. Sun, J. Wang, Synthesis of uniform WO_3 square nanoplates via an organic acid-assisted hydrothermal process, Materials Letters 6 (4) (2010) 1233.
[37] X.C. Song, Y.F. Zheng, E. Yang, Y. Wang, Large-scale hydrothermal synthesis of WO_3 nanowires in the presence of K_2SO_4, Materials Letters 61 (2007) 3905.
[38] X. Shen, G. Wang, D. Wexler, Large-scale synthesis and gas sensing application of vertically aligned and double-sided tungsten oxide nanorod arrays, Sensors and Actuators B: Chemical 143 (2009) 327.
[39] H.H. Nersisyan, W. Hyung, W.C. Whan, K.C. Cho, Combustion synthesis of nanostructured tungsten and its morphological study, Powder Technology 189 (2009) 422.
[40] M. Gillet, K. Masek, E. Gillet, Structure of tungsten oxide nanoclusters, Surface Science 566–568 (2004) 383.
[41] X.H. Xia, J.P. Tu, J. Zhang, X.H. Huang, X.L. Wang, X.B. Zhao, Fast electro-chromic properties of self-supported Co_3O_4 nanowire array film, Solar Energy Materials and Solar Cells 94 (2010) 386.
[42] B. Baloukas, J.M. Lamarre, L. Martinu, Electrochromic interference filters fabricated from dense and porous tungsten oxide films, Solar Energy Materials and Solar Cells 95 (2011) 807.
[43] X.H. Xia, J.P. Tu, J. Zhang, X.L. Wang, W.K. Zhang, H. Huang, Electrochromic properties of porous nickel oxide thin films prepared by a chemical bath deposition, Solar Energy Materials and Solar Cells 92 (2008) 628.
[44] X.H. Xia, J.P. Tu, J. Zhang, X.L. Wang, W.K. Zhang, H. Huang, Electrochromism in cobalt oxide marcobowl array films prepared by electrodeposition through monolayer polystyrene sphere template, ACS Applied Materials & Interfaces 2 (2010) 186.
[45] X.T. Su, F. Xiao, J.L. Lin, J.K. Jian, Y.N. Li, Q.J. Sun, J.D. Wang, Hydrothermal synthesis of uniform WO_3 submicrospheres using thiourea as an assistant agent, Materials Characterization 61 (2010) 831.
[46] B. Yang, P.R.F. Barnes, W. Bertram, V. Luca, Strong photoresponse of nanostructured tungsten trioxide films prepared via a sol–gel route, Journal of Materials Chemistry 17 (2007) 2722.
[47] M. Deepa, A.K. Srivastava, S.N. Sharma, Govind, S.M. Shivaprasad, Microstructural and electrochromic properties of tungsten oxide thin films produced by surfactant mediated electrodeposition, Applied Surface Science 254 (2008) 2342.
[48] S. Balaji, Y. Djaoued, A.S. Albert, R.Z. Ferguson, R. Bruning, Hexagonal tungsten oxide based electrochromic devices: spectroscopic evidence for the Li ion occupancy of four-coordinated square windows, Chemistry of Materials 21 (2009) 1381.
[49] Y.Z. Zhang, J.G. Yuan, J. Le, L.X. Song, X.F. Hu, Structural and electrochromic properties of tungsten oxide prepared by surfactant-assisted process, Solar Energy Materials and Solar Cells 93 (2009) 1338.
[50] L. Zhuang, X. Xu, H. Shen, A study on the gasochromic properties of WO_3 thin films, Surface and Coatings Technology 167 (2003) 217.
[51] B. Orel, U. Opara Krăsovec, N. Grŏselj, M. Kosec, G. Drazic, R. Reisfeld, Gasochromic behavior of sol–gel derived Pd doped peroxopolytungstic acid (W-PTA) nano-composite films, Journal of Sol-Gel Science and Technology 14 (1999) 291.
[52] S. Sekimoto, H. Nakagawa, S. Okazaki, K. Fukuda, S. Asakura, T. Shigemori, S. Takahashi, A fiber-optic evanescent-wave hydrogen gas sensor using palladium-supported tungsten oxide, Sensors and Actuators B: Chemical 66 (2000) 142.
[53] X.Q. Xu, H. Shen, X.Y. Xiong, Gasochromic effect of sol–gel WO_3–SiO_2 films with evaporated platinum catalyst, Thin Solid Films 415 (2002) 290.
[54] U.O. Krasovec, B. Orel, A. Georg, V. Wittwer, The gasochromic properties of sol–gel WO_3 films with sputtered Pt catalyst, Solar Energy 68 (2000) 541.
[55] B. Orel, N. Groselj, U.O. Krasovec, M. Gabrscek, P. Bukovec, R. Reisfeld, Gasochromic effect of palladium doped peroxopolytungstic acid films prepared by the sol–gel route, Sensors and Actuators B: Chemical 50 (1998) 234.
[56] A.H. Yan, C.S. Xie, D.W. Zeng, S.Z. Cai, H.Y. Li, Synthesis, formation mechanism and illuminated sensing properties of 3D WO_3 nanowall, Journal of Alloys and Compounds 495 (2010) 88.
[57] L.F. Cheng, X.T. Zhang, B. Liu, H.Z. Wang, Y.C. Li, Y.B. Huang, Z.L. Du, Template synthesis and characterization of WO_3/TiO_2 composite nanotubes, Nanotechnology 16 (2005) 1341.
[58] Y.C. Nah, A. Ghicov, D. Kim, P. Schmuki, Enhanced electrochromic properties of self-organized nanoporous WO_3, Electrochemistry Communications 10 (2008) 1777.
[59] J. Zhang, X.L. Wang, X.H. Xia, C.D. Gu, Z.J. Zhao, J.P. Tu, Enhanced electro-chromic performance of macroporous WO_3 films formed by anodic oxidation of DC-sputtered tungsten layers, Electrochimica Acta 55 (2010) 6953.
[60] L. Meda, R.C. Breitkopf, T.E. Haas, R.U. Kirss, Investigation of electrochromic properties of nanocrystalline tungsten oxide thin film, Thin Solid Films 402 (2002) 126.
[61] R. Deshpande, S.H. Lee, A.H. Mahan, P.A. Parilla, K.M. Jones, A.G. Norman, B. To, J.L. Blackburn, S. Mitra, A.C. Dillon, Optimization of crystalline tungsten oxide nanoparticles for improved electrochromic applications, Solid State Ionics 178 (2007) 895.

[62] B.B. Cao, J.J. Chen, X.J. Tang, W.L. Zhou, Growth of monoclinicWO_3 nanowire array for highly sensitive NO_2 detection, Journal of Materials Chemistry 19 (2009) 2323.
[63] W. Smith, Y.P. Zhao, Catalysis Communications 10 (2009) 1117.
[64] I. Porqueras, E. Bertran, Optical properties of Li^+ doped electrochromic WO thin films, Thin Solid Films 377–378 (2000) 8.
[65] A. Georg, W. Graf, R. Neumann, V. Wittwer, The role of water in gasochromic WO_3 films, Thin Solid Films 384 (2001) 269.
[66] R. Sivakumar, R. Gopalakrishnan, M. Jayachandran, C. Sanjeeviraja, Preparation and characterization of electron beam evaporated WO_3 thin films, Optical Materials 29 (2007) 679.
[67] H.S. Shim, J.W. Kim, Y.E. Sung, W.B. Kim, Electrochromic properties of tungsten oxide nanowires fabricated by electrospinning method, Solar Energy Materials and Solar Cells 93 (2009) 2062.
[68] Y.S. Lin, S.S. Wu, T.H. Tsai, Electrochromic properties of novel atmospheric pressure plasma jet-synthesized-organotungsten oxide films for flexible electrochromic devices, Solar Energy Materials and Solar Cells 94 (2010) 2283.
[69] J. Okumu, F. Koerfer, C. Salinga, T.P. Pedersen, M. Wuttig, Gasochromic switching of reactively sputtered molybdenumoxide films: a correlation between film properties and deposition pressure, Thin Solid Films 515 (2006) 1327.
[70] H. Shanak, H. Schmitt, J. Nowoczin, C. Ziebert, Effect of Pt-catalyst on gasochromic WO_3 films: optical, electrical and AFM investigations, Solid State Ionics 171 (2004) 99.
[71] M. Stolze, D. Gogova, L.K. Thomas, Analogy for the maximum obtainable colouration between electrochromic, gasochromic, and electrocolouration in DC-sputtered thin WO_{3-y} films, Thin Solid Films 476 (2005) 185.
[72] S.J. Ippolito, S. Kandasamy, K. Kalantar-zadeh, W. Wlodarski, Hydrogen sensing characteristics of WO_3 thin film conductometric sensors activated by Pt and Au catalysts, Sensors and Actuators B: Chemical 108 (2005) 154.
[73] A. Georg, W. Graf, R. Neumann, V. Wittwer, Stability of gasochromic WO_3 films, Solar Energy Materials and Solar Cells 63 (2000) 165.
[74] M. Ranjbar, N. Tahmasebi, G.S.M. Mahdavi, A. Irajizad, Electroless plating of palladiumon WO_3 films for gasochromic applications, Solar Energy Materials and Solar Cells 94 (2010) 201.
[75] K.J. Stevenson, J.T. Hupp, Microvisualization of structural features and ion electroinsertion behavior of patterned WO_3 thin films via integrated optical and atomic force microscopies, Solid-State Letters 2 (1999) 497.
[76] Y.S. Krasnov, G.Y. Kolbasov, Electrochromism and reversible changes in the position of fundamental absorption edge in cathodically deposited amorphous WO_3, Electrochimica Acta 49 (2004) 2425.
[77] J.J. Feng, J.J. Xu, H.Y. Chen, Direct electron transfer and electrocatalysis of hemoglobin adsorbed onto electrodeposited mesoporous tungsten oxide, Electrochemistry Communications 8 (2006) 77.
[78] B. Yang, H. Li, M. Blackford, V. Luca, Novel low density mesoporous WO_3 films prepared by electrodeposition, Current Applied Physics 6 (2006) 436.
[79] W.C. Hsu, C.C. Chan, C.H. Peng, C.C. Chang, Hydrogen sensing characteristics of an electrodeposited WO_3 thin film gasochromic sensor activated by Pt catalyst, Thin Solid Films 516 (2007) 407.
[80] W. Wei, Q. Yu, J. Lian, J. Bao, Z. Liu, S.S. Pei, Tetragonal tungsten oxide nanobelts synthesized by chemical vapor deposition, Journal of Crystal Growth 312 (2010) 3147.
[81] M. Gillet, R. Delamare, E. Gillet, Growth of epitaxial tungsten oxide nanorods, Journal of Crystal Growth 279 (2005) 93.
[82] K.A. Michalow, A. Heel, A. Vital, M. Amberg, G. Fortunato, K. Kowalski, T.J. Graule, M. Rekas, Effect of thermal treatment on the photocatalytic activity in visible light of TiO_2–W flame spray synthesised nanopowders, Topics in Catalysis 52 (2009) 1051.
[83] K.K. Akurati, A. Vital, J.P. Dellemann, K. Michalow, T. Graule, D. Ferri, A. Baiker, Flame-made WO_3/TiO_2 nanoparticles: relation between surface acidity, structure and photocatalytic activity, Applied Catalysis B: Environmental 79 (2008) 53.
[84] A.K.L. Sajjad, S. Shamaila, B. Tian, F. Chen, J. Zhang, One step activation of WO_x/TiO_2 nanocomposites with enhanced photocatalytic activity, Applied Catalysis B: Environmental 91 (2009) 397.
[85] C.F. Lin, C.H. Wu, Z.N. Onn, Degradation of 4-chlorophenol in TiO_2, WO_3, SnO_2, TiO_2/WO_3 and TiO_2/SnO_2 systems, Journal of Hazardous Materials 154 (2008) 1033.
[86] K.Y. Song, M.K. Park, Y.T. Kwon, H.W. Lee, W.J. Chung, W.I. Lee, Preparation of transparent particulate MoO_3/TiO_2 and WO_3/TiO_2 films and their photocatalytic properties, Chemistry of Materials 13 (2001) 2349.
[87] J.H. Pan, W.I. Lee, Preparation of highly ordered cubic mesoporous WO_3/TiO_2 films and their photocatalytic properties, Chemistry of Materials 18 (2006) 847.

Biographies

Ying Li received her MS degree in Department of Chemical Engineering and Biotechnology, National Taipei University of Technology (NTUT), Taipei, Taiwan. Presently she is PhD student in NTUT. Her research interests include development of biosensor, photoelectrocatalysis and biofuel cell. She has authored more than 10 research article published in international journals.

Pei-Chi Hsu received her BS degree in Department of Chemical and Materials Engineering, TamKang University, Taiwan. Presently she is master student in National Taipei University of Technology (NTUT), Taipei, Taiwan. Her research interests include development of photoelectrocatalysis based on TiO_2.

Shen-Ming Chen is a professor of Department of Chemical Engineering and Biotechnology, National Taipei University of Technology, Taipei, Taiwan. His main research interests are electroanalytical chemistry, bioelectrochemistry, photoelectrocatalysis, dye-sensitized solar cell (DSSCs) and biofuel cell. He has authored/coauthored more than 240 research article published in international journals.